IEEE Photonics Journal
An IEEE Photonics Society Publication



# A Multichannel Phase Tunable Microwave Photonic Mixer With High Conversion Gain and Elimination of Dispersion-Induced Power Fading

Volume 10, Number 1, February 2018

**Weile Zhai**
**Aijun Wen**, ***Senior Member, IEEE***
**Wu Zhang**
**Zhaoyang Tu**
**Huixing Zhang**
**Zhongguo Xiu**

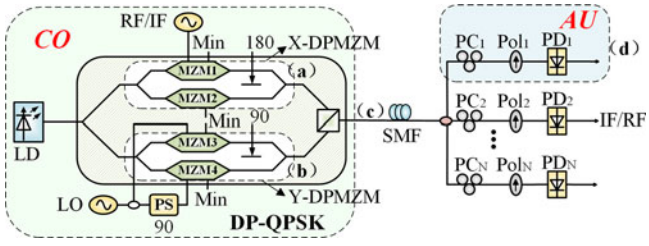


DOI: 10.1109/JPHOT.2017.2781238
1943-0655 © 2017 IEEE

# A Multichannel Phase Tunable Microwave Photonic Mixer With High Conversion Gain and Elimination of Dispersion-Induced Power Fading

**Weile Zhai,[1,2] Aijun Wen,[1,2] *Senior Member, IEEE*, Wu Zhang,[1,2] Zhaoyang Tu,[1,2] Huixing Zhang,[1,3] and Zhongguo Xiu[1,2]**

[1]State Key Laboratory of Integrated Service Networks, Xidian University, Xi'an 710071, China
[2]Collaborative Innovation Center of Information Sensing and Understanding, Xidian University, Xi'an 710071, China
[3]Department of Telecommunications Engineering, Xi'an 710071, China

*DOI:10.1109/JPHOT.2017.2781238*


Manuscript received November 15, 2017; revised December 5, 2017; accepted December 5, 2017. Date of publication December 13, 2017; date of current version January 3, 2018. This work was supported in part by the National Key Research and Development Program of China under Grant 2017YFB1104800, in part by the National Natural Science Foundation of China under Grant 61674119, in part by the National Postdoctoral Program For innovative Talents in China under Grant BX201600118, in part by the Young Talent fund of University Association for Science and Technology in Shaanxi, China, under Grant 20160109, in part by the project funded by China Postdoctoral Science Foundation under Grant 2017M613072, in part by the Natural Science Basic Research Plan in Shaanxi Province of China under Grant 2017JM6002, and in part by the Key Research and Development Program from Government of Shaanxi Province under Grant 2017GY-093. Corresponding author: Aijun Wen (e-mail: ajwen@xidian.edu.cn).

**Abstract:** A microwave photonic system that can realize frequency up- and down-conversion, multichannel phase shift, high conversion gain, and elimination of dispersion-induced power fading is proposed and experimentally demonstrated. The scheme is based on an integrated dual-polarization quadrature phase shift keying modulator that contains two dual parallel Mach–Zehnder modulators (X-DPMZM and Y-DPMZM). The X-DPMZM implements dual side band carrier suppression (DSB-CS) modulation of radio frequency signal, and the Y-DPMZM implements frequency shift of an optical carrier. They are combined in orthogonal polarizations to implement frequency up- and down-conversion. The polarization multiplexed signal will go through polarization controllers and polarizers to implement multi-channel phase shift. In the experiment, the phase shift can be tuned independently over 360° in each channel. By suppressing the optical carrier, the conversion gain and LO isolation are improved by 20.5 dB and 51.26 dB, respectively, compared with conventional dual side band modulation scheme. In addition, the proposed scheme can achieve a spurious-free dynamic range (SFDR) of 103.6 dB·Hz$^{2/3}$.

**Index Terms:** Microwave photonic mixer, phase shift, high conversion gain, dispersion-induced power fading, DP-QPSK modulator.

## 1. Introduction

The technique of beam forming plays an important role in communication systems, such as electronic countermeasure, phased array radar and sonar, etc. Especially in radar system, it can improve

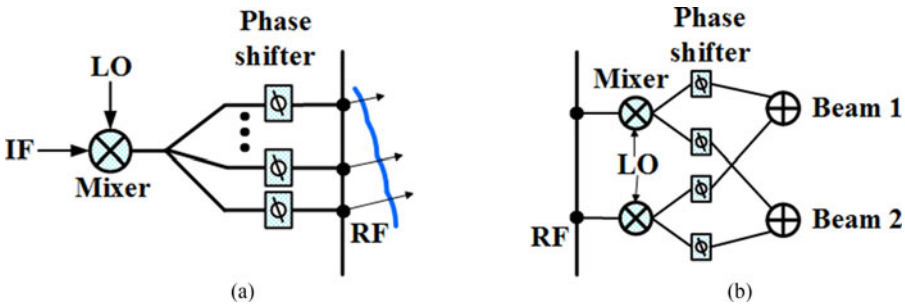


Fig. 1. (a) Beam forming for transmitter. (b) Multiple beam-forming for receiver.

anti-interference performance and detect the direction of signal source precisely. However, the electronic bottleneck limits the frequency and instantaneous bandwidth of radar system. Thanks to the large bandwidth, small size, light weight and immunity to electromagnetic interference (EMI) of the microwave photonics [1], beam forming based on microwave photonics has been intensively studied.

The two most important processing elements of beam forming are frequency converter and phase shifter [2], [3], [14]. There are various schemes of frequency conversion. The basic structure cascades two external intensity modulators. One of them is driven by radio frequency (RF) signal and the other is driven by local oscillation (LO) signal [4]. In order to achieve high conversion gain, schemes based on two modulators in parallel [5] or adjusting the DC bias to suppress the optical carrier have been proposed [5], [6]. Meanwhile, schemes with high linearity [7] and immunity to dispersion-induced power fading [8], [9] are also highly needed in modern communication system. Many other schemes are proposed to improve the performance of microwave photonic phase shift. A scheme which uses differential-group-delay element can achieve 360° phase shift over 40 GHz frequency range [10]. Wang et al came up with a scheme which can control the amplitude of the phase-shifted signal [11]. Zhang et al proposed a scheme based on dual-polarization quadrature phase shift keying (DP-QPSK) modulator to implement multichannel phase shift with frequency-multiplying [12].

However, the schemes mentioned before cannot achieve frequency conversion and phase shift in the same time, and both of them are indispensable for phased array radar. It is urgent to find a way to combine these two techniques and simplify the system. Recently, some new systems have been proposed. In [13], [14], a microwave photonic frequency down-conversion scheme with 360° phase shift have been reported. These schemes can be used in receiver for vector signal demodulation and beam forming. However, the use of optical band-pass filter limits the frequency tunability. To our knowledge, the optical filter with optimum performance is CVF-300CL/BVF-300CL from Alinar Labs [11]. The narrowest 3-dB bandwidth is 3.7 GHz and exhibits an ultra-sharp roll-off of 1500 dB/nm. But it still limits the minimum working frequency. On the other hand, the systems in [13], [14] cannot be applied in the transmitter because they cannot realize frequency up-conversion. In [15], a novel microwave mixer can achieve frequency up- and down-conversion with phase shift over 360°. But it also has two main shortcomings. One is that the scheme is sensitive to dispersion-induced power fading. The other is that the number of modulator will increase proportionally to implement multichannel frequency conversion with phase shift.

In this paper, we propose a multi-functional scheme which can achieve both frequency conversion and phase shift. Due to the single side band-carrier suppression (SSB-CS) modulation of local oscillation (LO) signal, it is immune to dispersion-induced power fading. The system possesses good frequency tunability without using optical filter and it has high conversion gain because of carrier suppression. Actually, if the 90° hybrid coupler with a frequency range from 8 to 67-GHz (Marki Microwave, QH-0867) is used, the operating frequency can be extended to U waveband [14]. The system can realize both beam forming and multiple beam-forming for both transmitter and receiver. Fig. 1(a) shows the beam forming for a transmitter. The IF signal experiences

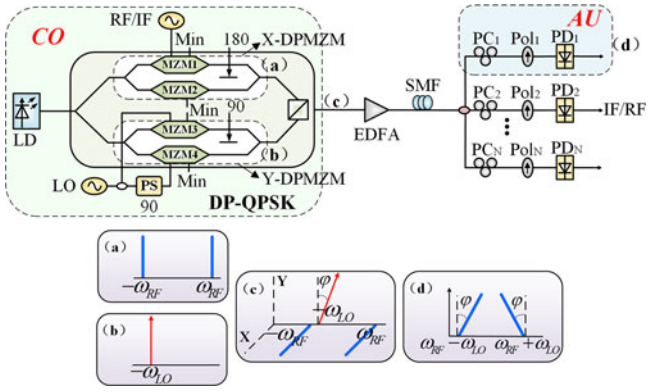


Fig. 2. System diagram of the microwave photonic mixer. LD, laser diode; DP-QPSK, dual polarization quadrature phase shifter keying modulator; LO, local oscillator; PS, phase shifter; PC, polarization controller; Pol, polarizer; PD, photo-detector; CO, center office; AU, antenna unit. (a)–(d) are the spectra at different location marked above.

frequency up-conversion and then is split into multiple channels to experience different phase shifts. Fig. 1(b) shows multiple beam-forming for a receiver. The RF signals received by multiple radiating elements experience frequency down-conversion and proper phase shift to form beam 1. Beam 2 can be formed with different phase shifts along different path in the same time [16]. So, our scheme can be widely used in beam forming for radar system and simplify the complexity of the system.

## 2. Principles

Fig. 2 shows the schematic diagram of proposed microwave photonic mixer. When an optical carrier from laser diode (LD) injects DP-QPSK modulator, it will be split into two parts and sent to X-DPMZM and Y-DPMZM. In our scheme, the output of X-DPMZM is dual side band-carrier suppression (DSB-CS) modulation of RF signal. The output of Y-DPMZM is SSB-CS modulation of LO signal, as shown in Fig. 2(a) and (b). They are combined in orthogonal polarizations by a polarization combiner (PBC) which is shown in Fig. 2(c). The polarization-multiplexed signal is split into several channels to implement multi-channel phase shift. In each channel, a polarization controller and a polarizer are employed. The phase difference between orthogonal signals can be tuned by polarization controller (PC). After optical-electrical conversion by photo-detector (PD), the microwave photonic mixer with phase-tunable ability is implemented.

The optical carrier from laser diode (LD) can be indicated as $E_{in}(t) = E_0 \exp(j\omega_c t)$,$E_0$ and $\omega_c$ represent the amplitude and angular frequency of the optical carrier, respectively. As can be seen from Fig. 2, the optical carrier injected into $MZM_1$ is modulated by RF signal. The RF signal can be expressed as $V(t) = V_{RF} \cos(\omega_{RF} t)$, where $V_{RF}$ and $\omega_{RF}$ represent the amplitude and angular frequency of the RF signal. $MZM_1$ and $MZM_2$ work at the minimum transmission point to suppress the optical carrier. There is some residual part of optical carrier due to the extinction ratio of the MZM. However, the main bias of X-DPMZM is also set at the minimum transmission point. As a result, the residual optical carrier of $MZM_1$ and $MZM_2$ can be cancelled. The output of $MZM_1$, $MZM_2$, and X-DPMZM can be given by

$$E_X(t) \approx \frac{E_{in}(t)}{4\sqrt{2}} j J_1(m_{RF}) [\exp(j\omega_{RF} t) + \exp(-j\omega_{RF} t)] \quad (1)$$

where $m_{RF} = \frac{V_{RF}}{V_\pi}\pi$ is the modulation index of RF signal and $J_n(\cdot)$ is the nth-order Bessel function of the first kind.

Similarly, $MZM_3$ is driven by LO signal and works at the minimum transmission point. $MZM_4$ is driven by the same LO signal with a 90° phase shift and also works at the minimum transmission point. The main bias of Y-DPMZM is set at the quadrature transmission point to implement SSB-CS modulation. The output of Y-DPMZM can be depicted as

$$E_Y(t) \approx \frac{E_{in}(t)}{2\sqrt{2}} jJ_1(m_{LO}) [\exp(-j\omega_{LO}t)] \tag{2}$$

where $m_{LO} = \frac{V_{LO}}{V_\pi}\pi$ is the modulation index of the LO signal.

As can be seen from Fig. 2(c), the output of X-DPMZM and Y-DPMZM are combined in orthogonal polarization states by PBC. The polarization-multiplexed optical signal at the output of the DP-QPSK modulator is given by

$$\begin{aligned} E_{DP-QPSK}(t) &= \begin{bmatrix} E_X(t) \\ E_Y(t) \end{bmatrix} \\ &= \frac{E_{in}(t)}{4\sqrt{2}} \begin{Bmatrix} jJ_1(m_{RF}) [\exp(j\omega_{RF}t) + \exp(-j\omega_{RF}t)] \\ 2jJ_1(m_{LO}) [\exp(-j\omega_{LO}t)] \end{Bmatrix} \end{aligned} \tag{3}$$

Then the modulated optical signal is split into each channel and goes through the PC and Pol, the polarization-multiplexed signal will be aligned into one polarization state. The output of the Pol is written as

$$\begin{aligned} E_{Pol-n}(t) &= \cos\theta \cdot E_X(t) + \sin\theta \cdot E_Y(t) \exp(j\varphi_n) \\ &= \frac{E_{in}(t)}{4\sqrt{2}} \begin{Bmatrix} \cos\theta \cdot jJ_1(m_{RF}) [\exp(j\omega_{RF}t) + \exp(-j\omega_{RF}t)] \\ + \sin\theta \cdot 2jJ_1(m_{LO}) [\exp(-j\omega_{LO}t)] \cdot \exp(j\varphi_n) \end{Bmatrix} \end{aligned} \tag{4}$$

As mentioned before, by adjusting the PC, the phase difference between the orthogonal signals can be tuned. In (4), $\varphi_n$ is the phase difference in the nth channel. We adjust PC to let the principle axes of the DP-QPSK modulator and the Pol have a 45 degree difference in polarization angle (The principle of PC can be seen in Appendix). After the photoelectric conversion in PD, the electric current can be expressed as

$$\begin{aligned} i_n(t) &= \eta \cdot E_{Pol-n}(t) \cdot E^*_{Pol-n}(t) \\ &= \eta \frac{E_0^2}{64} \cdot \begin{Bmatrix} J_1^2(m_{RF}) \cdot [2 + 2\cos(2\omega_{RF}t)] \\ + 4J_1^2(m_{LO}) \\ + 4J_1(m_{RF}) J_1(m_{LO}) [\cos((\omega_{RF} + \omega_{LO})t - \varphi_n) + \cos((\omega_{RF} - \omega_{LO})t + \varphi_n)] \end{Bmatrix} \end{aligned} \tag{5}$$

where $\eta$ is the responsivity of the photo-detector.

As can be seen from (5) and Fig. 2(d), the system can implement frequency up-conversion with the phase shift of $-\varphi_n$ and frequency down-conversion with the phase shift of $\varphi_n$. Meanwhile, the optical carrier which does not carry useful information is suppressed. So we can improve conversion gain by amplifying the modulated signal. In addition, since frequency conversion is based on SSB modulation, the system is immune to chromatic dispersion-induced power fading.

## 3. Experiments and Results

We set up an experiment according to the schematic diagram as shown in Fig. 2. A light wave from LD (Emcore, 1782) with the wavelength of 1552 nm is used as the optical carrier whose power is 17 dBm. The DP-QPSK modulator with an insertion loss of 13 dB (Fujitsu, FTM7977EX) has two DPMZMs in parallel. For each DPMZM, the half-wave voltage of each sub-modulator is about 3.5 V. An electrical phase shifter (ARRAL9428B, DC-18GHz) is utilized to make LO signal experience a 90-degree phase shift. An erbium-doped optical fiber amplifier (EDFA) (KPS-STD-BT-C-18-PB)

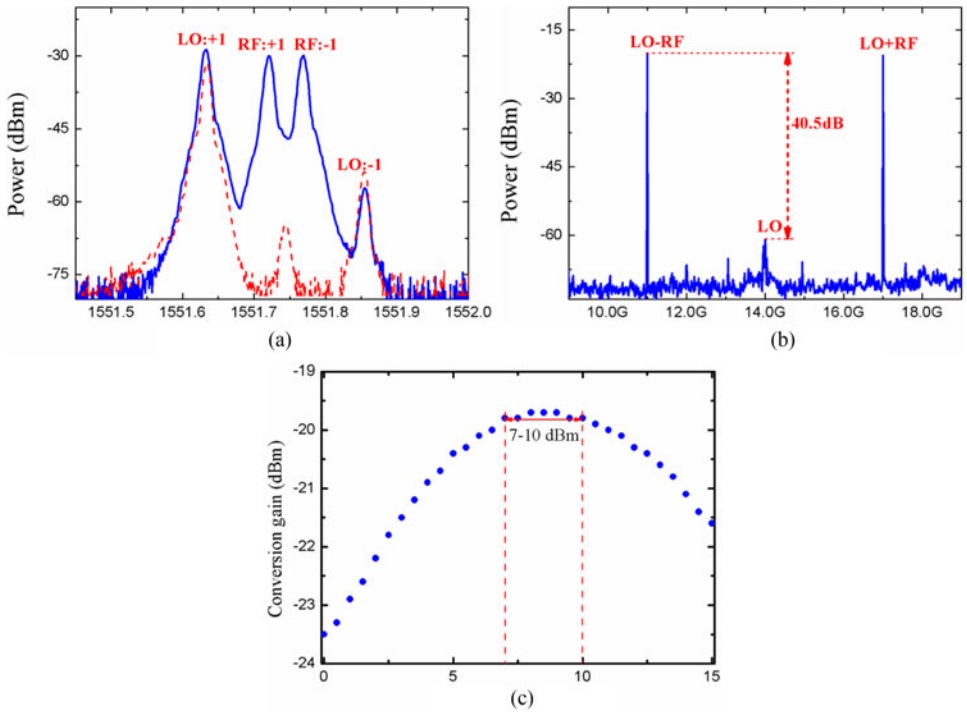


Fig. 3. (a) Optical spectrum at the output of DP-QPSK modulator in the proposed scheme (the power of LO signal is 10 dBm). (b) Electrical spectrum in the proposed scheme. (c) The conversion gain at different LO power while keeping the same optical power of 5 dBm into the PD.

which works at the automatic power control (APC) mode is used to amplify the weak signal after the DP-QPSK modulator. The output power of EDFA is 16 dBm, which ensures the average power injected into PD is 5 dBm.

Firstly, we demonstrate the performance of frequency conversion. As shown in Fig. 2, $MZM_1$ is driven by RF signal with the frequency of 3 GHz and the power of 0 dBm which is generated by an analog signal source (Rohde & Schwarz SMW200A); $MZM_3$ is driven by LO signal with the frequency of 14 GHz generated by another analog signal source (Agilent, N5183A) and $MZM_4$ is driven by the same LO signal with a 90-degree phase shift. The output of DP-QPSK modulator is the combination of DSB-CS modulation of RF signal and SSB-CS modulation of LO signal, as shown in Fig. 3(a). The $+1$st-order sideband of LO is suppressed for almost 30 dB. However, due to the limited spectral resolution of the optical spectrum analyzer (Adantest, Q8384, 0.01 nm), the rejection level of the optical carrier cannot be clearly observed. So, we measure the optical spectrum without injecting the RF signal, as shown in Fig. 3(a) red dashed line. After the optical signal is detected by PD, electrical spectrum is obtained and given in Fig. 3(b). The LO-IF isolation reaches 40.5 dB and the power of output IF signal is $-19.1$ dBm. Note that the conversion gain is defined as the ratio of the output frequency converted signal power and the input RF signal power. Because of the power of RF signal in the experiment is 0 dBm, the power of output IF frequency signal is just the conversion gain, which means the conversion gain in our scheme is $-19.1$ dB, In the experiment, we adjust the power of LO to obtain the max conversion gain [17]. As can be seen from Fig. 3(c), as the LO power changes from 0 dBm to 15 dBm, the conversion gain increase first and then decrease. When the power of LO signal is in the range of 7–10 dBm, the conversion gain will reach to $-19.7$ dB.

In order to explain high conversion gain clearly, we set a matched group which does not suppress the optical carrier. The optical and electrical spectra are shown in Fig. 4. Similarly, the power injected into PD is 5 dBm. As displayed in Fig. 4(a), the optical carrier occupy the main power of signal,

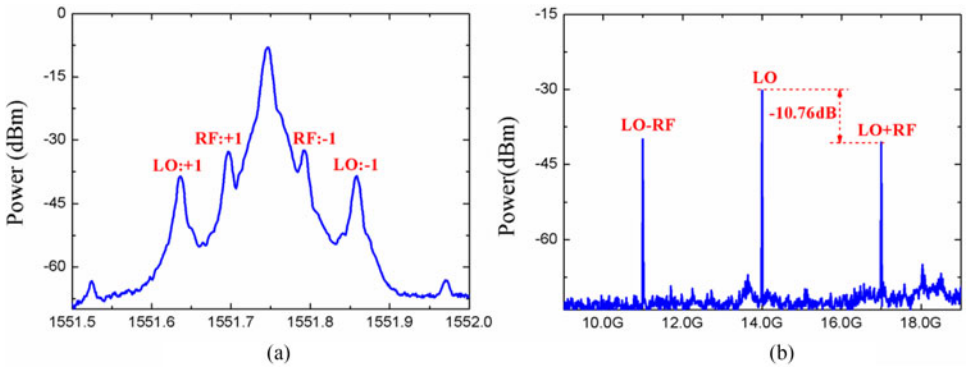


Fig. 4. (a) Optical spectrum at the output of DP-QPSK modulator in the conventional DSB modulation scheme. (b) Electrical spectrum in the conventional DSB modulation scheme.

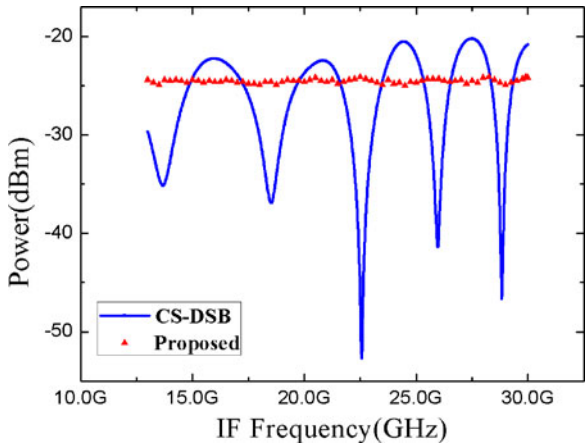


Fig. 5. Measured and simulation IF power as carrier frequency changes from 3 to 20 GHz.

resulting in two main problems. Firstly, as displayed in Fig. 4(b), the power of detected IF signal is only −39.6 dBm, which means the conversion gain is just −39.6 dBm. Secondly, the LO-IF isolation is only 10.76 dB. Comparing Fig. 3(b) and Fig. 4(b), our scheme can realize 20.5 dB improvement in conversion gain and 51.26 dB in LO-IF isolation.

Next, we measure the influence of fiber dispersion. We use a 50-km single mode fiber whose dispersion coefficient is about 16 ps/nm/km. A 100 Mbaud 16 quadrature amplitude modulation (16-QAM) signal generated from vector signal generator (Rohde & Schwarz, SMW200A) is modulated on a 3 GHz-carrier signal. The power of the IF signal is recorded when the carrier frequency changes from 3 to 20 GHz. The results are shown in Fig. 5. To compare with the conventional DSB-CS modulation scheme, the corresponding theoretical curve is also plotted. In the proposed scheme, the power of the IF signal remains unchanged when the carrier frequency changes. However, for DSB-CS modulation scheme, the power of IF signal declines periodically. Furthermore, we measure the constellation diagram of proposed scheme and DSB-CS modulation scheme as shown in Fig. 6(a) and (b). There is about 11% improvement in EVM.

Meanwhile, SFDR is measured in the experiment. A two-tone RF signal with the frequency of 5 GHz and 5.2 GHz are generated from analog signal sources (Rohde & Schwarz SMW200A; Agilent N5183A). And LO signal with the frequency of 16 GHz is generated from an analog signal source (Agilent 83630B). So, the frequency of the up-conversion fundamental terms are 21 GHz and 21.2 GHz. The frequency of the up-conversion third-order intermodulation distortion are 20.8 GHz

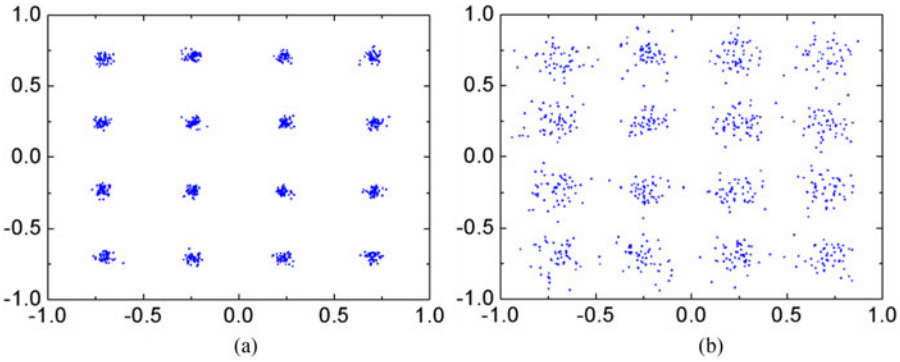


Fig. 6. (a) Constellation diagram of propose scheme. (b) Constellation diagram of conventional DSB-CS modulation scheme.

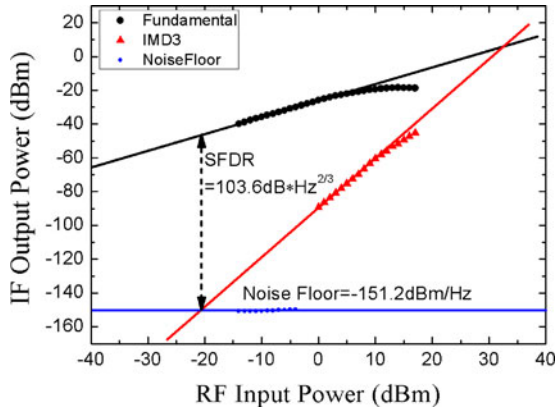


Fig. 7. Measured power of up-conversion fundamental term, up-conversion third-order intermodulation distortion and noise floor after PD. SFDR: Spurious Free Dynamic range.

and 21.4 GHz. In the experiment, as we change the power of the input RF signal, the power of Noise floor, up-conversion fundamental term and third-order intermodulation distortion are recorded. As can be seen from Fig. 7, the SFDR of proposed scheme is 103.6 dB·Hz$^{2/3}$.

Finally, the phase of the IF signal is demonstrated. It should be noted that the best device to measure the phase shift is vector network analyzer. Limited by the condition of our laboratory, we use an oscilloscope (Tektronix, MDO3102) with the bandwidth of 1 GHz, sample rate of 5 G Samples/sec. Therefore, we can only measure the phase for down-conversion signal. As can be seen from Fig. 2(d), the phase shift for up-conversion signal and down-conversion signal is just opposite. For frequency down-conversion with phase shift, a 16.1 GHz RF sinusoidal-signal is down-converted to 100-MHz IF signal by mixing it with a 16 GHz LO single-tone signal. Meanwhile, RF signal is down-converted to 100-MHz IF signal by an electrical mixer (CMB43431009H) and this IF signal is used as a standard signal. Then, the two down-conversion signals inject the dual-channel oscilloscope. CH1 is the standard signal and CH2 is the signal with different phase shift. Fig. 8 shows the IF signal waveforms with phase shift of 0–360° with a step of 45°. So, our scheme can achieve continuous phase shift over 360 degrees. Moreover, the amplitude of phase-shifted IF signals remain almost unchanged. As mentioned before, for each channel, the phase shift is realized by adjusting the polarization state of modulated signal by PC independently. The tuning rate and stability can be improved by replacing the three-paddle PC with electrically controlled PC [18]. The result manifests that our scheme can be used in beam forming for both transmitter and receiver.

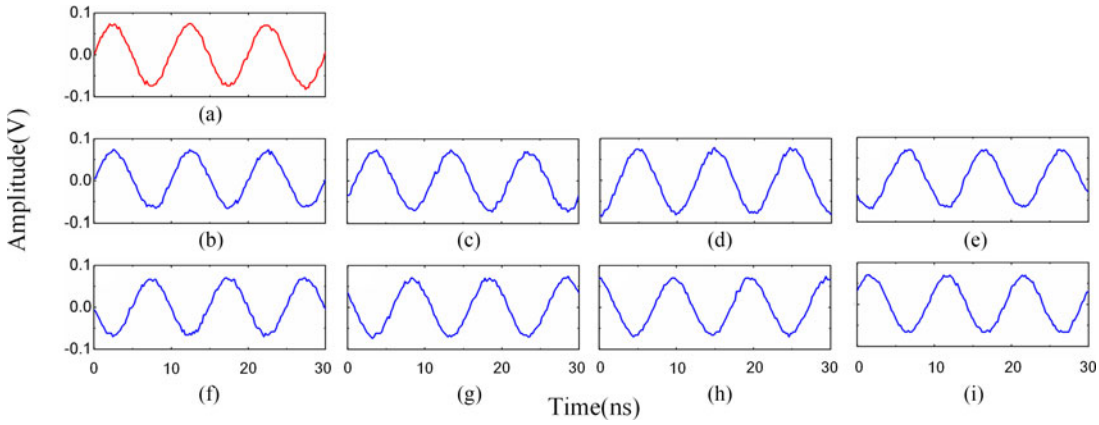


Fig. 8. (a) is the waveform of standard IF signal in CH1; (b)–(i) are the waveforms of phase-shifted IF signal with phase shift of 0°, 45°, 90°, 135°, 180°, 225°, 270° and 315°.

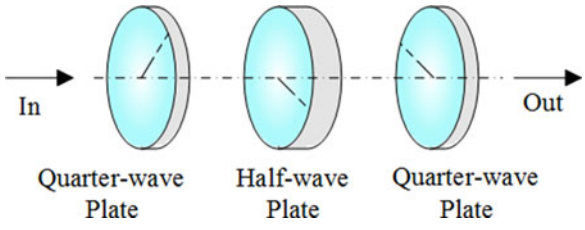


Fig. 9. A three wave plates polarization controller.

## 4. Conclusion

In conclusion, a multifunctional microwave photonic mixer with high performance is proposed and experimentally demonstrated. It can realize both frequency up- and down-conversion with continuous 360° phase shift in a wide frequency range when high performance commercial 90° hybrid coupler is adopted. Thanks to the carrier suppression technology, the conversion gain improves by 20.5 dB compared with DSB modulation scheme. What's more, the scheme is immune to dispersion-induced power fading and the ability of multichannel phase shift can simplify the system of beam forming in both transmitter and receiver.

## Appendix

Fig. 9 is the structure of a typical PC, it contains two quarter-wave plates (QWP) and one half-wave plate (HWP). The wave plate has two orthogonal optical axes, which are called fast axis and slow axis (as shown in Fig. 10). When a light-wave goes through the wave plate, it will introduce a phase difference $\varphi$ between two light vectors in fast axis and slow axis [19].

Assuming that X-axis and Y-axis are two main axes of a input light wave, the input light vector is expressed as $(A_1, B_1)$. When light $(A_1, B_1)$ goes through the wave plate, the components in fast axis and slow axis are written as C and D.

$$\begin{aligned} C &= A_1 \cos\theta + B_1 \sin\theta \\ D &= (B_1 \cos\theta - A_1 \sin\theta) \exp(j\varphi) \end{aligned} \tag{6}$$

Where $\theta$ is the angle between fast axis and X-axis, as shown in Fig. 10. The projections of $A_1$ and $B_1$ in X-axis and Y-axis are the output light vector $(A_2, B_2)$.

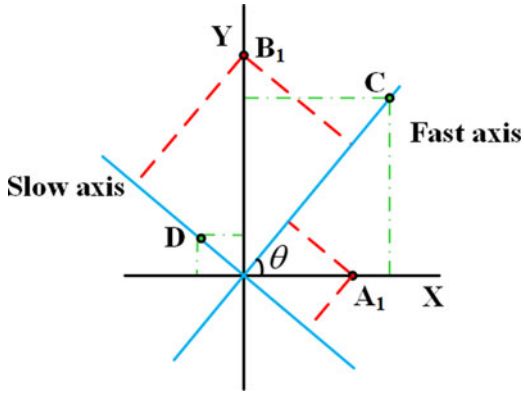


Fig. 10. The vector diagram of the light which goes through a wave plate.

$$\begin{aligned} A_2 &= C \cdot \cos\theta - D \cdot \sin\theta \\ &= A_1\left(\cos^2\theta + \sin^2\theta \exp\left(j\varphi\right)\right) + B_1\left(\sin\theta\cos\theta - \cos\theta\sin\theta\exp\left(j\varphi\right)\right) \\ B_2 &= C \cdot \sin\theta + D \cdot \cos\theta \\ &= A_1\left(\sin\theta\cos\theta - \cos\theta\sin\theta\exp\left(j\varphi\right)\right) + B_1\left(\sin^2\theta + \cos^2\theta\exp\left(j\varphi\right)\right) \end{aligned} \tag{7}$$

As a result, The transformation Jones matrix of the wave plate can be expressed as

$$J_{WP}\left(\varphi,\theta\right) = \begin{bmatrix} \cos\frac{\varphi}{2} + j\sin\frac{\varphi}{2}\cos 2\theta, & -j\sin\frac{\varphi}{2}\sin 2\theta \\ -j\sin\frac{\varphi}{2}\sin 2\theta, & \cos\frac{\varphi}{2} - j\sin\frac{\varphi}{2}\cos 2\theta \end{bmatrix} \cdot \exp\left(j\frac{\varphi}{2}\right) \tag{8}$$

We can get the transformation Jones matrix of a QHQ type PC by multiplexing the transformation matrix of three wave plates [20]

$$\begin{aligned} J_{PC} &= J_{QWP}\left(\frac{\pi}{2},\theta_1\right)\cdot J_{HWP}\left(\pi,\theta_2\right)\cdot J_{QWP}\left(\frac{\pi}{2},\theta_3\right) \\ &= \begin{bmatrix} \frac{\sqrt{2}}{2} + j\frac{\sqrt{2}}{2}\cos 2\theta_1, & -j\frac{\sqrt{2}}{2}\sin 2\theta_1 \\ -j\frac{\sqrt{2}}{2}\sin 2\theta_1, & \frac{\sqrt{2}}{2} - j\frac{\sqrt{2}}{2}\cos 2\theta_1 \end{bmatrix} \cdot \begin{bmatrix} j\cos 2\theta_2 & , & -j\sin 2\theta_2 \\ -j\sin 2\theta_2 & , & -j\cos 2\theta_2 \end{bmatrix} \\ &\quad \cdot \begin{bmatrix} \frac{\sqrt{2}}{2} + j\frac{\sqrt{2}}{2}\cos 2\theta_3, & -j\frac{\sqrt{2}}{2}\sin 2\theta_3 \\ -j\frac{\sqrt{2}}{2}\sin 2\theta_3, & \frac{\sqrt{2}}{2} - j\frac{\sqrt{2}}{2}\cos 2\theta_3 \end{bmatrix} \\ &= \frac{1}{2}\begin{bmatrix} -\cos\left(2\theta_1 - 2\theta_2\right) - \cos\left(2\theta_2 - 2\theta_3\right) - j\cos\left(2\theta_1 - 2\theta_2 + 2\theta_3\right) + j\cos 2\theta_2, \\ -\sin\left(2\theta_1 - 2\theta_2\right) - \sin\left(2\theta_2 - 2\theta_3\right) + j\sin\left(2\theta_1 - 2\theta_2 + 2\theta_3\right) - j\sin 2\theta_2 \\ \sin\left(2\theta_1 - 2\theta_2\right) + \sin\left(2\theta_2 - 2\theta_3\right) + j\sin\left(2\theta_1 - 2\theta_2 + 2\theta_3\right) - j\sin 2\theta_2, \\ -\cos\left(2\theta_1 - 2\theta_2\right) - \cos\left(2\theta_2 - 2\theta_3\right) + j\cos\left(2\theta_1 - 2\theta_2 + 2\theta_3\right) - j\cos 2\theta_2 \end{bmatrix} \end{aligned} \tag{9}$$

When (10) satisfies the condition

$$\begin{aligned} 2\theta_1 - 2\theta_2 &= -\left(2\theta_2 - 2\theta_3\right) \Rightarrow \theta_1 = \theta_3 \\ 2\theta_1 - 2\theta_2 + 2\theta_3 &= \left(2k+1\right)\pi - 2\theta_2 \Rightarrow \theta_1 + \theta_3 = \frac{\left(2k+1\right)\pi}{2} \qquad k = 0, 1 \end{aligned} \tag{10}$$

Equation (10) can be simplified as

$$J_{PC} = \begin{bmatrix} \exp\left(j\left(2\theta_2 + \frac{\pi}{2}\right)\right), & 0 \\ 0, & \exp\left(-j\left(2\theta_2 + \frac{\pi}{2}\right)\right) \end{bmatrix} \tag{11}$$

As can be seen from (11), when a light goes through the PC, the phase difference between the two orthogonal polarization states can be tuned over 360 degrees with the amplitude of the input light unchanged. In practical operation, we keep the first and the third wave plates to be stationary at $\frac{\pi}{4}$ (or $\frac{3\pi}{4}$), and tune the phase shift by adjusting the second plate.

## References


[1] A. Altaqui, E. H. Chan, and R. A. Minasian, "Microwave photonic mixer with high spurious-free dynamic range," *Appl. Opt.*, vol. 53, no. 17, pp. 3687–3695, Jun. 2014.

[2] J. F. Coward, C. H. Chalfant, and P. H. Chang, "A photonic integrated-optic RF phase shifter for phased array antenna beam-forming applications," *J. Lightw. Technol.*, vol. 11, no. 12, pp. 2201–2205, Dec. 1993.

[3] R. Benjamin, C. D. Zaglanikis, and A. J. Seeds, "Optical beam former for phased arrays with independent control of radiated frequency and phase," *Electron. Lett.*, vol. 26, no. 22, pp. 1853–1855, Oct. 1990.

[4] G. K. Gopalakrishnan, W. K. Burns, and C. H. Bulmer, "Microwave-optical mixing in $LiNbO_3$ modulators," *IEEE Trans. Microw. Theory Tech.*, vol. 41, no. 12, pp. 2383–2391, Dec. 1993.

[5] E. H. W. Chan and R. A. Minasian, "Microwave photonic downconverter with high conversion efficiency," *J. Lightw. Technol.*, vol. 30, no. 23, pp. 3580–3585, Dec. 2012.

[6] W. Zhang, A. Wen, and Y. Gao, "Microwave photonic frequency conversion with high conversion efficiency and elimination of dispersion-induced power fading," *IEEE Photon. J.*, vol. 8, no. 3, May 2016, Art. no. 5500909.

[7] W. Li and J. Yao, "Dynamic range improvement of a microwave photonic link based on bi-directional use of a polarization modulator in a Sagnac loop," *Opt. Exp.*, vol. 21, no. 13, pp. 15692–15697, Jun. 2013.

[8] Y. Gao, A. Wen, and X. Wu, "Efficient photonic microwave mixer with compensation of the chromatic dispersion-induced power fading," *J. Lightw. Technol.*, vol. 34, no. 14, pp. 3440–3448, Apr. 2016.

[9] S. Li, X. Zheng, H. Zhang, and B. Zhou, "Compensation of dispersion-induced power fading for highly linear radio-over-fiber link using carrier phase-shifted double sideband modulation," *Opt. Lett.*, vol. 36, no. 4, pp. 546–548, Feb. 2011.

[10] Z. Li, C. Yu, and Y. Dong, "Linear photonic radio frequency phase shifter using a differential-group-delay element and an optical phase modulator," *Opt. Lett.*, vol. 35, no. 11, pp. 1881–1883, May 2010.

[11] X. Wang, J. Zhang, E. H. W. Chan, X. Feng, and B.-O. Guan, "Ultra-wide bandwidth photonic microwave phase shifter with amplitude control function," *Opt. Exp.*, vol. 25, no. 3, pp. 2883–2894, Feb. 2017.

[12] Y. Zhang and S. Pan, "Frequency-multiplying microwave photonic phase shifter for independent multichannel phase shift," *Opt. Lett.*, vol. 41, no. 6, pp. 1261–1264, Mar. 2016.

[13] Y. Gao, A. Wen, and Z. Tu, "Simultaneously photonic frequency downconversion, multichannel phase shift, and IQ demodulation for wideband microwave signals," *Opt. Lett.*, vol. 41, no. 19, pp. 4484–4487, Sep. 2016.

[14] T. Jiang, S. Yu, and R. Wu, "Photonic downconversion with tunable wideband phase shift," *Opt. Lett.*, vol. 41, no. 11, pp. 2640–2643, Jun. 2016.

[15] T. Jiang, R. Wu, and S. Yu, "Microwave photonic phase-tunable mixer," *Opt. Exp.*, vol. 25, no. 4, pp. 4519–4527, Feb. 2017.

[16] P. W. Delaney, "An RF multiple beam-forming technique," *IRE Trans. Mil. Electron.*, vol. 6, no. 12, pp. 179–186, Apr. 1962.

[17] Z. Tang and S. Pan, "A reconfigurable photonic microwave mixer using a 90° optical hybrid," *IEEE Trans. Microw. Theory Tech.*, vol. 64, no. 9, pp. 3017–3025, Aug. 2016.

[18] Y. Gao, A. Wen, and H. Zheng, "Photonic microwave waveform generation based on phase modulation and tunable dispersion," *Opt. Exp.*, vol. 24, no. 12, pp. 12524–12533, May 2016.

[19] F. Heismann, "Analysis of a reset-free polarization controller for fast automatic polarization stabilization in fiber-optic transmission systems," *J. Lightw. Technol.*, vol. 12, no. 4, pp. 690–699, Apr. 1994.

[20] N. Liu *et al.*, "A novel photonic RF phase shifter based on polarization controller," *Microw. Opt. Technol. Lett.*, vol. 52, no. 11, pp. 2598–2600, 2010.